



Palladium nanoparticles supported on amine-functionalized alginate foams for hydrogenation of 3-nitrophenol

Shengye Wang, Yayuan Mo, Thierry Vincent, Jean-Claude Roux, Enrique Rodríguez-Castellón, Catherine Faur, Eric Guibal

► To cite this version:

Shengye Wang, Yayuan Mo, Thierry Vincent, Jean-Claude Roux, Enrique Rodríguez-Castellón, et al.. Palladium nanoparticles supported on amine-functionalized alginate foams for hydrogenation of 3-nitrophenol. *Journal of Materials Science*, 2020, 55 (5), pp.2032-2051. 10.1007/s10853-019-04099-y . hal-02366009

HAL Id: hal-02366009

<https://hal.umontpellier.fr/hal-02366009>

Submitted on 23 May 2022

HAL is a multi-disciplinary open access archive for the deposit and dissemination of scientific research documents, whether they are published or not. The documents may come from teaching and research institutions in France or abroad, or from public or private research centers.

L'archive ouverte pluridisciplinaire **HAL**, est destinée au dépôt et à la diffusion de documents scientifiques de niveau recherche, publiés ou non, émanant des établissements d'enseignement et de recherche français ou étrangers, des laboratoires publics ou privés.

Palladium nanoparticles supported on amine-functionalized alginate foams for hydrogenation of 3-nitrophenol

Shengye Wang^{1,2}, Yayuan Mo¹, Thierry Vincent¹, Jean-Claude Roux¹, Enrique Rodríguez-Castellón³, Catherine Faur⁴, and Eric Guibal¹

¹ C2MA, IMT Mines Ales, Univ Montpellier, Ales, France

² Department of Environmental Engineering, College of Chemistry and Environmental Engineering, Shenzhen University, Shenzhen, People's Republic of China

³ Departamento de Química Inorgánica, Facultad de Ciencias, Universidad de Málaga, Málaga, Spain

⁴ IEM, Institut Européen des Membranes, Univ Montpellier, CNRS, ENSCM, Montpellier, France

ABSTRACT

A new material, consisting of alginate–polyethyleneimine (AP) foam, with high percolating properties has been designed for palladium recovery in fixed-bed reactor. The foam, having high affinity for Pd(II), can be also used for manufacturing heterogeneous hydrogenation catalyst. SEM–EDX and TEM analyses were performed to determine the structure of the foams and the distribution of Pd nanoparticles (after metal reduction). Metal-sorbent interactions and oxidation state of Pd are characterized by XPS. Pd(0)-bearing foams are investigated for the hydrogenation of 3-nitrophenol (3-NP) using HCOOH as the hydrogen donor. The maximum sorption capacity of Pd(II) by AP foams reaches up to 224 mg g⁻¹. The water flux (under water-depth pressure of 6 mbar) reaches 24.8 mL cm⁻² min⁻¹ (superficial flow velocity: 14.9 m h⁻¹). The foams are remarkably stable: The mass loss under strong shaking for 2 days does not exceed 3%. For catalytic application, Pd loading conditions were optimized (flow rate, metal concentration) to reach 101 mg Pd g⁻¹ (97% metal removal). Under these conditions, Pd overloading and nanoparticles aggregation can be minimized. The catalytic hydrogenation of 3-nitrophenol (using formic acid as the hydrogen donor) was optimum for a HCOOH/3-NP molar ratio close to 160 (pH between 3 and 4). High flow rates minimize diffusion effects; the apparent rate constant (for pseudo-first-order rate equation) reaches 9.7 × 10⁻³ s⁻¹. The reuse of the foams over 30 cycles shows the long-term stability of catalytic activity. The test on continuous (one-pass) mode shows a progressive poisoning of the catalyst. However, a simple washing with water is sufficient for recovering catalytic activity.

Introduction

The use of platinum group metals (PGMs) has attracted increasing attention during the last decades due to their outstanding catalytic properties. Palladium, in particular, has been the basis for producing electronic devices and automotive catalysts owing to its high catalytic activity for various chemical reactions. Previous studies have fully reported the use of metal nanoparticles for methylene blue removal [1], nitrophenol hydrogenation [2–5], formaldehyde degradation [6], etc. One of the major drawbacks of Pd for catalytic applications is associated with its high cost. Therefore, recovering precious metals (including Pd) from waste resources is becoming an important industrial challenge. Many studies have been focusing on the recovery of Pd(II) from acidic leachates of waste catalysts [7]. On the other hand, there is still much scope left for improving its application potential as catalysts. For example, the aggregation and poor reusability of palladium nanoparticles still limit their use. Therefore, a stabilizer is commonly needed to enhance the stability of the palladium nanoparticles [8]. Those stabilizers can be inorganic or organic supports that may have moderate affinity toward metal nanoparticles. To date, nanoparticles were mostly immobilized in inorganic supports such as SDS-intercalated LDH [9], magnetic supports [10], mesoporous silica, zeolites and activated carbon [11]. Unfortunately, it is easy for the metal nanoparticles immobilized on those inorganic supports to leach out during reaction process [12]. Moreover, the reuse of nanoparticles is still limited since recovery techniques are typically energy intensive and laborious. Conventional separation processes such as filtration not only make the treatment procedure more time-consuming, but also easily cause catalyst loss [13]. One possible way to solve this problem is to decorate the catalyst in magnetic materials [14]. Another way may consist of applying polymers as the supports owing to their simplified synthesis, good stability and easy recovery [15, 16].

Alginate is a natural biopolymer extracted from seaweeds. One of the advantages of applying alginate is that this material is versatile in terms of shaping and conditioning owing to gelation processes. It can be shaped into nanoparticles [17], gel beads [18–20], membranes [21, 22], fibers [23] and foams [24] for

various applications in different fields. More specifically, alginate has demonstrated its efficiency as immobilizers (through alginate–Ca gelation) for nanoparticles, such as Ag and Au [25], Ni/Fe [26], Pd [27] and Fe_2O_3 [28]. Polyethyleneimine (PEI) is well known for its metal chelating characteristic owing to the presence of a large number of amine groups (primary, secondary and tertiary amine groups, in branched PEI). Therefore, alginate–Ca/PEI composite can both coordinate with Pd nanoparticles and act as stabilizer for these nanoparticles. In addition, a post-treatment using glutaraldehyde (GA) may contribute to strengthen the alginate–Ca/PEI composite. The Schiff-base reaction between PEI and GA prevents the degradation of alginate–Ca/PEI composite in complex systems with an excess of ions such as K(I) or Na(I) (usually due to the formation of soluble Na-alginate or K-alginate, etc.). Actually, the simultaneous cross-linking mechanisms between interpenetrating polymers lead to stable complex structures. This method has been recently applied to elaborate alginate/PEI beads for Pd(II) binding immobilization of Pd [29], and nanoparticles on alginate/PEI-GA beads in our group. However, although the catalyst is recoverable owing to its large size (around 3 mm) and stable even in complex systems, its catalytic activity for 3-nitrophenol hydrogenation is much lower than the values reported for more conventional catalysts due to poor mass transfer property. Compared to conventional shaking or agitating systems, the use of a fixed-bed column system could enable continuous water treatment by feeding the wastewater at one side of the reactor and obtaining the treated water from the other end. In the case of large and homogeneous (in size and shape) support, the natural percolation of the liquid into the packing makes the process very effective from a mass transfer point of view. Another advantage of this system is that it requires no solid–liquid separation after treatment. A specific shaping of the catalysts (such as macroporous foams) would be favorable for application in this kind of system, avoiding head loss and clogging effects. Therefore, a highly porous foam-like support is highly required to (a) decrease the mass transfer resistance, (b) simplify the reaction equipment and (c) improve the reaction rate.

To address these requirements, highly porous foams that exhibit outstanding percolating characteristics are synthesized. For the first time, the foams are prepared through the reaction between alginate

and partially protonated PEI solution. The challenge also consisted of using a very simple air-drying process for conditioning the foams instead of more sophisticated drying processes (such as freeze-drying or drying under supercritical CO₂ conditions). To prevent air-drying shrinkage that might cause cracks and water tightness of the foams, the foam was cross-linked with GA solution: Aldehyde functions react with free amine groups on PEI. The as-prepared foams are packed in tubular reactors and tested for Pd(II) recovery from acidic solution. In a second step, metal-loaded foams are used for manufacturing catalysts by in situ reduction of loaded Pd(II) into Pd(0). The hydrogenation of nitrophenol is an ideal model reaction to assess the catalytic activity of a variety of metallic nanoparticles. In addition, nitrophenol is considered as highly toxic organic pollutant in industrial wastewater or agricultural runoff and its reduced product (3-aminophenol, 3-AP) is an important intermediate for producing antipyretic drugs. Therefore, the hydrogenation of 3-NP by formic acid was used as a model reaction to evaluate the catalytic activity of the catalysts. Nitrophenol is reported to be easily reduced to aminophenol by NaBH₄ in the presence of metals in solution; the metal nanoparticles catalyze this reaction by facilitating electron relay from the donor BH₄⁻ to acceptor (nitrophenol) to overcome the kinetic barrier. However, to avoid using the toxic and high-cost NaBH₄ chemical in the water treatment process, the hydrogen donor was replaced by formic acid, since this reagent is non-toxic and can be handled and stored easily [30]. Gowda et al. [31] reported that formic acid in the presence of 10% Pd-C is a rapid, versatile and selective reducing system for a wide range of nitro compounds. Therefore, this study aims to evaluate the possibility of using novel alginate/PEI foams as a stabilizer for Pd nanoparticles and determine the catalytic activity of the catalyst packed in tubular reactors for 3-NP hydrogenation by HCOOH. The first part of the work characterizes the materials using techniques such as SEM, TEM, XPS analyses and physical measurements of porosity, water flux and stability under agitation. In the second part, the study focuses on the influence of a series of experimental parameters (pH, metal content on the catalyst, molar ratio between the feed and the hydrogen donor, i.e., HCOOH) on the kinetics of hydrogenation of 3-nitrophenol.

Materials and method

Materials

Manugel GMB alginate was obtained from FMC BioPolymer (Girvan, UK). Branched polyethyleneimine (PEI, 50% (w/w) in water), formic acid (99%) and glutaraldehyde (GA, 50% (w/w) in water) were purchased from Sigma-Aldrich (Taufkirchen, Germany). Nitric acid (65% w/w) and palladium(II) chloride were obtained from R.D.H (Seelze, Germany). Hydrazine hydrate N₂H₄·H₂O (reagent grade, 55% ± 5%) was purchased from Sigma-Aldrich (Taufkirchen, Germany), and 3-nitrophenol (3-NP) was supplied by Fluka (Buchs, Switzerland). The metal stock solution was prepared by dissolving 1 g of PdCl₂ in 1 L of 1.1 M HCl solution, while 3-nitrophenol stock solution was prepared by dissolving 1 g into 1 L of water with 1 drop of NaOH solution (≈ 0.1 mL, 10 M).

Preparation of foams

Figure S1 (see Supplementary Information, SI) shows the process for preparing alginate/PEI (AP) foams. Briefly, one hundred milliliters of 4% alginate solution were first mixed with 400 mL of water. Thereafter, 35 mL of 4% PEI (dissolved in slightly acidic nitric acid solutions) were slowly added into the solution while agitating. The mixture was then poured into a container and maintained at 20 ± 1 °C for 24 h for completing the gelation. Varying the size of containers allows manufacturing foams with different thicknesses. After that, the foam was washed 4 times using deionized water, added with 2.5 mL of GA (50%, w/w) and maintained at 20 ± 1 °C for 24 h. Finally, the foam was thoroughly washed and air-dried at 20 ± 1 °C.

Immobilization of Pd(II)

Figure S2 (see SI) shows the experimental setup used for metal sorption: The foam was cut into cylinders using a cutter mold and packed in a plastic tube that was fixed above a container filled with the Pd(II) solution. The solution was recirculated through the foam using a peristaltic pump (Ismatec, ISM 404, Wertheim, Germany) for 24 h. When the height of the water column is around 0.5 cm, the lid is then tightened to seal the recirculation system to maintain a

constant water pressure on the foam (constant level of solution at the top of the column). Time starts when the first drop reaches the foam. The sorption isotherm experiment was conducted using solutions containing different concentrations of Pd(II). One liter of solution (at pH 1, controlled with H_2SO_4) was recirculated through AP foam. Specifically, to study the effect of Pd(II)-loaded amount, 1 L of Pd(II) solution at different concentrations (i.e., 10–50 mg Pd L^{-1}) was recirculated through a foam disk (255 mg, dried weight). The flow rate of the pump was set at 30 mL min^{-1} . The effect of flow rate was studied by the contact of 1 L of Pd(II) solution (28 mg L^{-1}) with 255 mg of the foam at three different flow rates (i.e., 5, 30 and 50 mL min^{-1}). For the effect of foam mass, three different masses of the foam cylinders with the same diameter (2.43 cm) but different heights were applied for Pd(II) recovery from solutions containing a concentration of 28 mg Pd L^{-1} . The flow rate was fixed at 50 mL min^{-1} .

Reduction of Pd(II) into Pd(0)

Before reduction, the Pd(II)-loaded foams were thoroughly washed. A previous study showed that a small size (~ 3 nm) of Pd nanoparticles could be obtained by reduction with hydrazine hydrate ($\text{N}_2\text{H}_4\cdot\text{H}_2\text{O}$) in alkaline solution [32]. Therefore, in this study, the reduction of Pd(II) to Pd(0) loaded on the foams was performed by gentle stirring (50 mov/min) in a solution (200 mL) containing freshly prepared hydrazine hydrate (0.03 M) and NaOH (0.5 mM) at 60 °C for 5 h. The color of the foams changed from yellowish brown to dark gray, suggesting the formation of metallic palladium nanoparticles on the surface of the foams.

Characterization of materials

Scanning electron microscopy (SEM) and SEM-EDX (SEM coupled with energy-dispersive X-ray diffraction analysis) were performed using an environmental scanning electron microscope Quanta FEG 200 (FEI France, Thermo Fisher Scientific, Mérégnac, France), equipped with an Oxford Inca 350 energy-dispersive X-ray micro-analyzer (Oxford Instruments France, Saclay, France). TEM micrographs were obtained on the SEM using the TEM-emulation mode. Materials were grinded, sieved (below 250 μm) and dispersed in an ethanol solution. A

micro-drop of the homogenous suspension was deposited at the surface of a grid C film (S160, 200 mesh Ni grid, Agar Scientific, Stansted, UK). XPS studies were carried on a Physical Electronics spectrometer (PHI Versa Probe II Scanning XPS Microprobe, Physical Electronics, Chanhassen, MN, USA) with monochromatic X-ray Al K_α radiation (100 μm , 100 W, 20 kV, 1486.6 eV) and a dual-beam charge neutralizer. The spectrometer energy scale was calibrated using Cu $2p_{3/2}$, Ag $3d_{5/2}$ and Au $4f_{7/2}$ photoelectron lines at 932.7 eV, 368.2 eV and 84.0 eV, respectively. Under a constant pass energy mode at 23.5 eV condition, the Au $4f_{7/2}$ line was recorded with 0.73 eV FWHM at a binding energy (BE) of 84.0 eV. XPS spectra were analyzed using PHI SmartSoft software and processed using MultiPak 9.3 package. The binding energy values were referenced to adventitious carbon C 1s signal (284.8 eV). Recorded spectra were systematically fitted using Gauss–Lorentz curves. Atomic concentration percentages of the characteristic elements of the surfaces were determined taking into account the corresponding area sensitivity factor for the different measured spectral regions. Samples were finely grinded (below 125 μm) to get an analysis representative of the whole mass of the materials.

The apparent density and porosity of the foams were measured by pycnometer method using ethanol as a soaking agent. Water flux ($\text{mL cm}^{-2} \text{min}^{-1}$) was calculated from the flux at a unit time on a unit foam area (the height of the foams was maintained at 8.0 ± 0.2 mm); the pressure calculated from the water height was 0.006 bar (calculated by the depth of the water on the top of the foam). The pH_{PZC} of the foams was measured by titration method. Two hundred milligrams of sorbent were mixed with 40 mL of 0.1 M NaCl solution for 48 h; the initial pH values (pH_0) were adjusted between 2 and 10 using a pH meter (inoLab pH 7110, WTW, Germany). The final pH (pH_{eq}) was recorded and plotted against initial pH; the pH_{PZC} corresponds to the pH where the plot crosses the first bisector (i.e., $\text{pH}_{\text{eq}} = \text{pH}_0$). Stability of the foams was determined by recording the mass of AP foam before (around 255 mg, dry weight) and after shaking in water at 150 rpm for 2 days. The mass loss (%) was calculated after the drying of the structured foam.

Catalytic hydrogenation of 3-nitrophenol

For 3-nitrophenol (3-NP) hydrogenation, the catalyst was also packed in the reactor shown in Figure S2 (See SI). Unless specified, 3-NP was reduced by recirculating the 3-NP solution (100 mL, 50 mg L⁻¹) containing 0.2% formic acid through the catalyst disk (weight: 255 ± 10 mg). Samples were collected and acidified with sulfuric acid (1 mL sample with 20 µL 5% H₂SO₄) before being analyzed using a UV spectrophotometer (Shimadzu UV-1650PC, Kyoto, Japan) at 332 nm [33]. According to a previous study [34], the hydrogenation of 3-NP by formic acid can be expressed as Scheme S1 (see SI). Different parameters may influence the conversion of 3-NP into 3-AP (3-aminophenol), such as the pH of the solution (controlled by NaOH or HNO₃), the molar ratio between the hydrogen donor and the feed (HCOOH/3-NP), and the flow rate. The reuse of the catalyst was also investigated for 30 cycles. Full experimental conditions are systematically reported in the caption of figures.

Statistical analysis

Selected experiments were duplicated. Average values and standard deviations were calculated. Moreover, 3-NP hydrogenation using catalysts prepared from different foams was carried out to evaluate the reproducibility of the manufacturing procedure. The overlapped plots shown in Figure S3 (see SI) indicate that the synthesis of AP/Pd catalyst is reproducible.

Results and discussion

Characterization of materials

Foam stability (mechanical agitation) and physicochemical properties

Table 1 gives the measured values of several physicochemical properties of the foams before and after metal loading process. The pH_{PZC} is 6.29 for raw AP foams. At pH < pH_{PZC}, positively charged surface of AP foams can attract the chloro-anionic species of palladium [35]. The apparent density is 0.0637 g cm⁻³; after sorption, it increases up to 0.0644 g cm⁻³, which is probably related to more compact structure of the foams (see SEM images,

Fig. 1). Therefore, Pd(II)-loaded AP foam also presents a slightly lower porosity than the raw material. Despite strong shaking, both free and metal-loaded foams maintain a low mass loss around 3%; this high stability enables the reusability of AP/Pd catalyst. The stability of Pd nanoparticles on the catalyst is a key criterion for designing a heterogeneous catalyst. For example, Vincent et al. [35] reported the beneficial use of ionic liquid for stabilizing palladium in alginate-based catalysts (Pd(II) being reduced after binding to the ionic liquid immobilized in alginate capsules): The strong interaction between phosphonium cation and anionic chloropalladate species prevents the leaching of palladium and increase the life of the catalyst.

The BET analysis of the foam is not reported here. Preliminary tests show that specific surface area (SSA) does not exceed 2–3 m² g⁻¹. This means that the hyper-macroporous material has limited micro/mesoporosity (which would contribute to the SSA). Complementary tests (not shown) conclude that a final drying under more sophisticated drying conditions (freeze-drying or drying under supercritical CO₂ conditions) did not significantly changed the SSA.

Morphological observations

SEM imaging (Fig. 1) shows the interconnected porous network: It is randomly distributed on the surface and the vertical section of the raw foams, contributing to their high percolating properties. After loading Pd(II), the pore wall of the foams becomes more compact. This result is in agreement with the decrease in porosity and water flux after the sorption process. This change in structure could be due to the pressure of the circulation sorption system and the re-drying process after metal sorption. In addition, the reaction of amine groups with anionic chloropalladate species may contribute to form additional interchain bonds. EDX analysis mainly shows the presence of C and O elements. The resolution and the sensitivity are not sufficient to achieve the identification of N peak within the forest of peaks (including C and O strong peaks), despite the presence of numerous amine functions on PEI. After Pd(II) sorption, a large peak of Pd is found in/on the foams. The semiquantitative analysis shows that the surface of the catalyst bears up to 17.7% (w/w) of palladium, while the metals reach up to 18.9% in the

Table 1 Physicochemical characteristics of raw and Pd(II)-loaded AP foams

Properties	AP foam	Pd(II)-loaded AP foam
pH _{PZC}	6.29	—
Water flux (mL cm ⁻² min ⁻¹)	24.81 ± 0.48	19.27 ± 1.34
Porosity (%)	70.93 ± 1.60	69.79 ± 0.22
Density (g cm ⁻³)	0.0637 ± 0.0005	0.0644 ± 0.0005
Stability (mass loss, %)	2.98 ± 0.14	2.91 ± 0.26

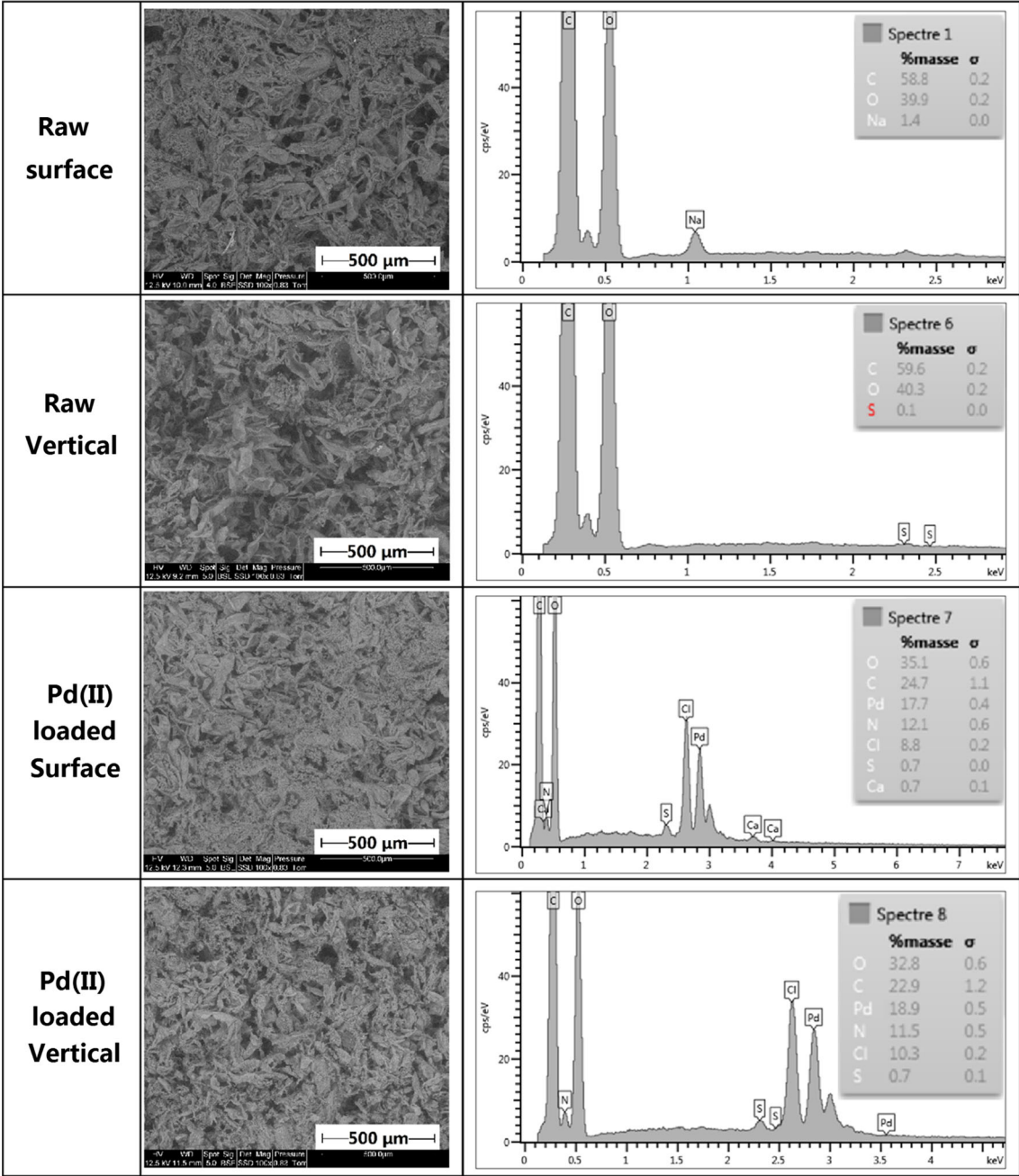


Figure 1 SEM-EDX micrographs of raw and Pd(II)-loaded foams.

internal part of the material: The catalyst is homogeneous in terms of distribution of Pd. The EDX element mapping (Figure S4, see SI) further confirms that the Pd(II) is well dispersed. Besides, Cl element appears in the foams. This can be the first evidence that Pd(II) is bound under the form of chloro-palladium complexes. A small amount of S element is also detected (0.7%), because the pH was adjusted using H_2SO_4 and SO_4^{2-} /or HSO_4^- and could also bind to protonated amine groups. The semiquantitative analysis of Pd should simply be considered indicative. Indeed, the mass balance on Pd concentrations before and after sorption shows much lower values (27.2 mg Pd loaded on 255 mg of foam; after sorption and metal reduction, the final weight is close to 308 mg; i.e., Pd loading close to 8.8%, w/w).

Sizing of Pd nanoparticles on the catalytic foams

The high-magnification mode on SEM allows observing (a) the presence of Pd(II) (the high atomic weight of Pd gives a good contrast for identifying the localization of metal binding zones at the surface of the material), and (b) the distribution of Pd nanoparticles (small spots). Figure 2a shows the rugged surface of Pd(II)-loaded AP foams. After reduction using hydrazine hydrate, Pd(II) is, at least partially, converted into Pd nanoparticles (small spots in Fig. 2b, of lower individual surface area than the surface area of Pd(II)-loaded zones, in Fig. 2a). It is noteworthy that these nanoparticles are remarkably well distributed; this can be explained by the good dispersion of PEI in the alginate/PEI material. Similar trends were observed for algal/PEI beads catalysts: When PEI is incorporated as GA cross-linked microparticles, the distribution of small Pd nanoparticles is less homogenous than when the algal beads were impregnated with PEI (before being cross-linked with GA) [36].

Despite a few aggregates of individual Pd nanoparticles, the TEM images presented in Fig. 2c again confirm the good dispersion of these particles. The size of Pd particles (shown in Fig. 2d) mainly ranges between 4.5 and 10.5 nm (i.e., average value: 7.61 ± 1.93 nm), slightly larger than those free particles previously reported [37, 38]; however, with the advantage of immobilization for a readily recycling or reuse. It was reported that Pd nanoparticles with size ranging between 6 and 8 nm are appropriate for alkene hydrogenation reactions [39].

XPS characterization: modes of interaction and oxidation states of Pd

Figure 3 shows the XPS survey of the materials (raw foam, AP; AP after Pd(II) loading; AP-Pd(II); AP-Pd(II) reduced, as the catalyst; and catalyst after 30 cycles of usage). The survey curves confirm the presence of N element (as a marker for PEI incorporation) and O element (marker of the biopolymer). The sorption of Pd is characterized by the characteristic signals of Pd 3d bands (and additional weaker signals, such as Pd 4p, Pd 3p, Pd 3s or Pd MNN). It is noteworthy that after Pd(II) sorption the sorbent bears chloride ions (Cl 2p signal); this means that at least a significant fraction of Pd(II) is bound as chlorocomplex (probably as chloroanionic species). After reduction (and also after 30 cycles of use), the intensity of this signal is drastically reduced (almost disappearing). Figures S5–S8 (see SI) report the HRES spectra for specific C 1 s, O 1 s, N 1 s, Pd 3d and Cl 2p. Table S1 (see SI) summarizes the main deconvoluted bands for these signals, their assignments and their relative fractions for (a) identifying the binding mechanisms, (b) the effective reduction of Pd(II) into Pd(0) and (c) evaluating the stability of the catalyst after intensive use.

The XPS analysis of AP sorbent confirms the presence of carboxylate groups (both on C 1s and O 1s signals) and amine and quaternary ammonium groups (399.1 eV (71%) and 401.1 eV (29%), respectively). The protonation of amine groups and the quaternary ammonium sites are favorable for the sorption of anionic species (such as chloroanionic species). After Pd(II) sorption, the appearance of chlorine element confirms the binding of these chloroanionic Pd species on the sorbent; a third band associated with N element appears as the bond between N and Pd. This is also confirmed by the coexistence of two pairs of deconvoluted bands (Pd $3d_{5/2}$ and Pd $3d_{3/2}$) for Pd 3d signal corresponding to Pd–N (about 40%), Pd–Cl (about 60%) bonds. After Pd(II) reduction on the sorbent (synthesis of Pd(0) supported catalyst), the N 1s core-level spectrum is very close to the spectrum for AP material (though the peak at high BE is now appearing as N–Pd species rather than the ammonium form). It is noteworthy that the C 1 s signal loses its symmetry for the two highest bands, representative of adventitious C, C–C and –C=C– that increases comparatively to the second band representative of C–OH, C–O–C and C–N

Figure 2 SEM micrographs of **a** Pd(II) loaded and **b** surface of Pd nanoparticles-loaded foams, **c** TEM micrographs of Pd nanoparticles-loaded foams and **d** size distribution of Pd particles.

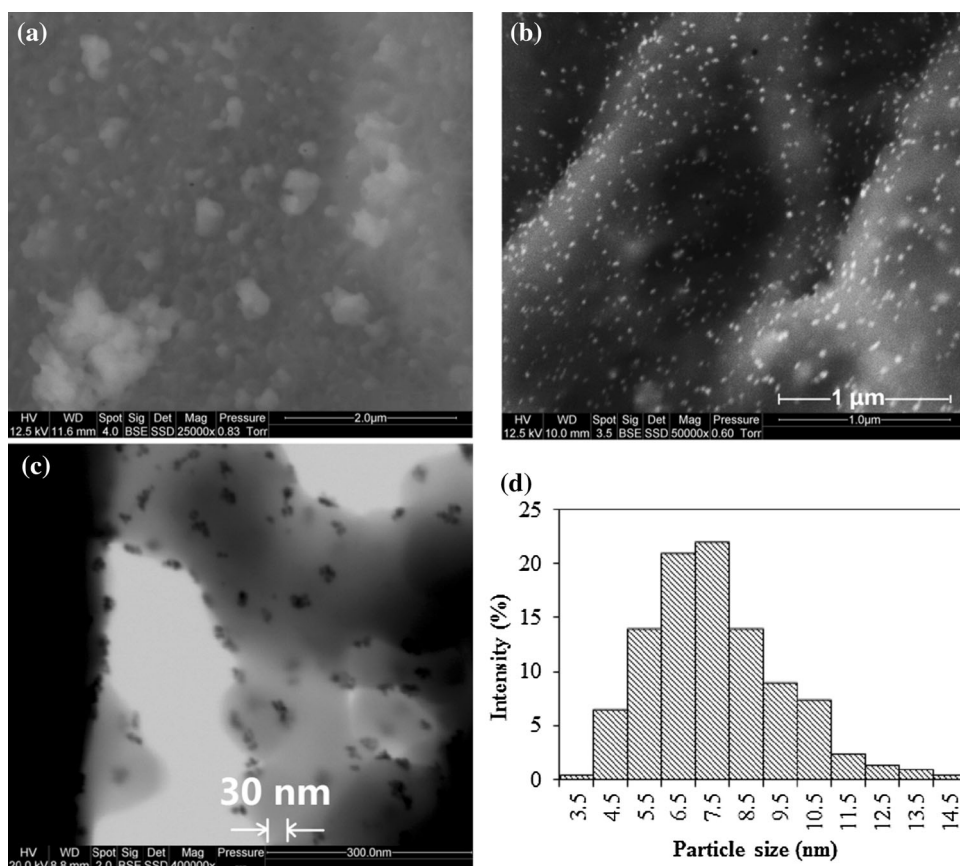
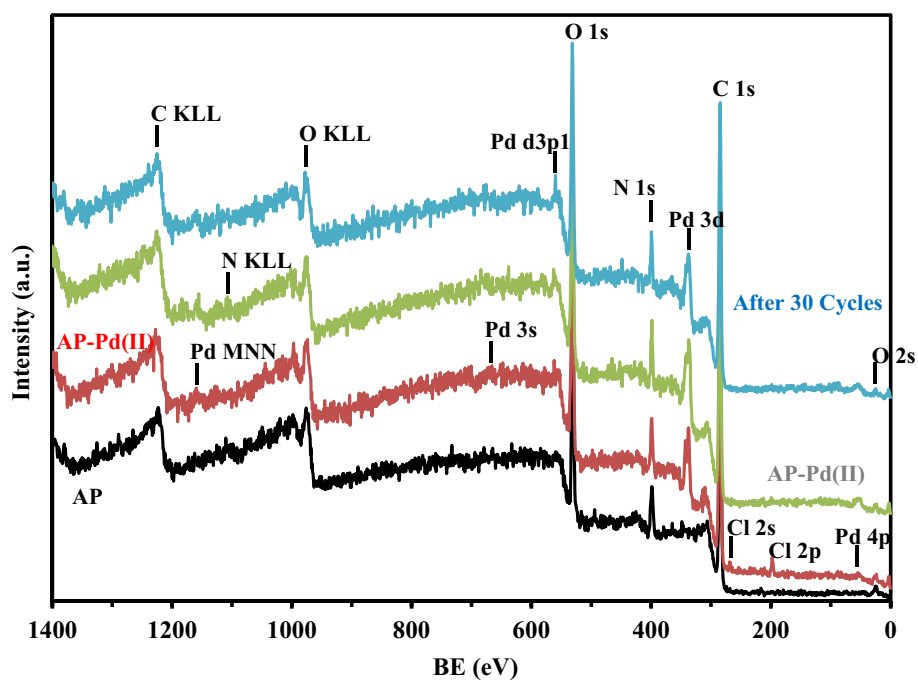


Figure 3 XPS survey analysis of AP, AP-Pd(II), AP-Pd(II) Reduced (catalyst) and catalyst after 30 cycles.



chemical groups. This probably means that the reduction conditions affect the chemical environment of these functional groups (including a possible

reductive action on these groups). The intensity of Cl 2p signal strongly decreased, and it was not possible getting a clear identification of the bands: The

reduction releases chloride by conversion of PdCl_4^{2-} species into $\text{Pd}(0)$. Obviously, the reduction is characterized by the appearance of a new band for $\text{Pd } 3d$: The signal is deconvoluted in 3 pairs of bands corresponding to Pd-Cl (28%), Pd-N (28%) and $\text{Pd}(0)$ (44%) forms. This means that the reduction of $\text{Pd}(\text{II})$ is only partial. This may affect the catalytic activity of the foam. The comparison of the XPS spectra for the different bands between AP- $\text{Pd}(\text{II})$ reduced and catalyst after 30 cycles shows that the profiles are roughly comparable: This is a clear demonstration of the stability of the support. The main differences are essentially identified in terms of relative fractions: distribution between $-\text{NH}$ and N-Pd forms and a little decrease in the proportion of $\text{Pd}(0)$ (from 44 to 37%).

These results show some trends:

- Metal binding occurs through electrostatic attraction/ion exchange between protonated amine groups (of PEI) and chloroanionic Pd species.
- A partial reduction of $\text{Pd}(\text{II})$ happens (limited to 44%).
- There is a relative chemical stability of the AP- $\text{Pd}(0)$ after 30 cycles of use.

Catalytic activity: effect of experimental parameters

Effect of Pd loading

Previous studies have suggested that the incorporation of PEI significantly improves the sorption capacity for $\text{Pd}(\text{II})$ from acidic solution owing to the abundant amine groups on this material. Thus, the alginate/PEI foam is not only potentially a stabilizer for Pd nanoparticles, but also a potential sorbent for $\text{Pd}(\text{II})$ recovery. To test the sorption property of AP foams for $\text{Pd}(\text{II})$ from acidic solution, the sorption isotherms were carried out by recirculating solutions containing different concentrations of $\text{Pd}(\text{II})$ through a fixed mass of AP foam. It is noteworthy that, due to the amount of hydrochloric acid (1.1 M) in the stock solution, the predominant palladium species in those diluted working solutions is PdCl_4^{2-} . Figure S9 (see SI) shows that the maximum sorption capacity reaches up to $223.6 \text{ mg Pd g}^{-1}$. The partial protonation of amine groups makes the sorbent cationic at mild acid pH and then capable of binding chloro-

anions. The eventual coexistence of free amine groups might also contribute to bind uncharged or free $\text{Pd}(\text{II})$ species; nevertheless, the strong predominance of chloro-anionic species limits the relevance of this mechanism. Table S2 (see SI) reports $\text{Pd}(\text{II})$ sorption properties for a variety of materials. In general, phenolic hydroxyl group-based materials such as tannin show the lowest sorption capacity among the listed materials. The sorption mechanism was reported as a combination of ligand substitution and redox reaction [40]. The raw algal biomass that contains a certain amount of amine and carboxyl groups shows comparable (slightly higher) sorption property compared to tannin. Amine group-based chitosan derivatives and aminated alginate and algal beads possess the highest sorption capacities; these materials can bind chloro-palladium complexes from acidic solution through electrostatic attraction [41] or coordinate to palladium(II) in neutral solution [42]. Owing to the abundant amine groups brought by PEI and the higher accessibility of the sorption sites on porous AP foams, especially compared to polymer beads, the foams present much higher sorption capacity than other listed materials. This outstanding affinity of the foams for $\text{Pd}(\text{II})$ is critical for improving the stability of Pd nanoparticles immobilized on this support. Indeed, a strong binding contributes to reduce metal leaching during the catalytic cycle; this is especially important for the development of efficient heterogeneous catalysts.

Contrary to other nanoparticles, Pd nanoparticles immobilized on the foams offer opportunities for application in fixed-bed column system in either recirculation mode or one-pass mode. Since $\text{Pd}(\text{II})$ is in situ reduced into $\text{Pd}(0)$ on the foams, the different conditions during loading process may lead to a change in distribution of Pd nanoparticles on the supports and thus affect the catalytic performance. Therefore, the effect of Pd loading amount, flow rate and foam height during loading process was firstly studied in recirculation mode. The Pd loading amount is one of the most critical factors that markedly affect catalytic activity [43]. To study the effect of Pd loading amount, solutions with different initial $\text{Pd}(\text{II})$ concentrations (11, 16, 21, 28 and 52 mg L^{-1}) were recirculated through the foam (weight: $255 \pm 10 \text{ mg}$). The recovery efficiencies are 100, 99.8, 98.5, 97.1 and 71%, respectively, and the corresponding sorption capacities are 43.8, 67.7, 84.0, 110.4 and 154.5 mg g^{-1} , respectively.

After metal reduction, these as-prepared catalysts loaded with different Pd amounts were compared for 3-NP hydrogenation. A controlled experiment was performed with the raw foam. As shown in Fig. 4a, the concentration of 3-NP is not significantly reduced with the raw foam, indicating that the hydrogenation of 3-NP is negligible in the absence of the active phase and that the sorption of the contaminant onto the foams is also limited. Despite a slight decrease when applying foams loaded with 11 mg or 16 mg Pd, their plots almost overlap with the kinetic profile obtained with the raw material. When the amount of Pd increases to 21 mg or higher, the concentration of 3-NP decreases significantly with increasing reaction time; however, the reason causes such a sharp improvement of hydrogenation efficiency remains unclear. The hydrogenation completely converts 3-NP into 3-AP within 10 min, showing the marked catalytic performance of AP/Pd catalyst.

The pseudo-first-order rate equation (PFORE) and the pseudo-second-order rate equation (PSORE) are commonly used for describing homogeneous chemical reactions. In the case of heterogeneous reactions, the contribution of resistances to bulk, film and intraparticle diffusions affects the overall kinetics. These simplified equations have been also used for modeling heterogeneous reactions such as sorption or supported catalysis. However, in these cases the rate coefficients should be considered as apparent rate coefficients. In the present study, the large excess of hydrogen donor compared with the substrate makes its concentration almost unchanged and the

reaction rate will artificially depend only on the concentration of the substrate (apparent mononuclear reaction). This means that the hydrogenation of 3-NP will preferentially be described by the PFORE (Eq. 1). Complementary tests on modeling kinetic profiles with the PSORE confirmed poor fitting of experimental data.

$$-\frac{dC}{dt} = k_1 C \quad (1a)$$

$$\text{Integrated to } \ln \frac{C_t}{C_0} = -k_1 t \quad (1b)$$

where k_1 (min^{-1}) is the rate coefficient for PFORE and C_0 (and C_t) is the initial substrate concentration (and the residual concentration of the substrate at time t).

To verify this hypothesis, $\ln(C_t/C_0)$ was plotted against reaction time (Fig. 4b). The fine linear relationship confirms that this model is appropriate to describe the kinetics. To compare the catalytic efficiencies, the apparent rate constants (k , s^{-1}) and the catalytic activity ($k_{\text{Pd}} = k/m_{\text{Pd}}$; $\text{s}^{-1} \text{g}^{-1}$) were calculated. Due to its lowest number of Pd sites, AP/Pd_{21mg} has the slowest reaction with k value close to $6.52 \times 10^{-3} \text{ s}^{-1}$. When the loading Pd amount grows by 6 mg, the reaction constant rate increases to $8.18 \times 10^{-3} \text{ s}^{-1}$. Further increase in the Pd content from 27 mg to 37 mg does not significantly change the rate constant. Similar result was reported by Jadbabaei et al. [44], who concluded that a higher Pd content does not necessarily result in higher catalytic activity, and the optimum Pd loading amount (i.e., the lowest Pd amount without sacrificing reactivity) is when the

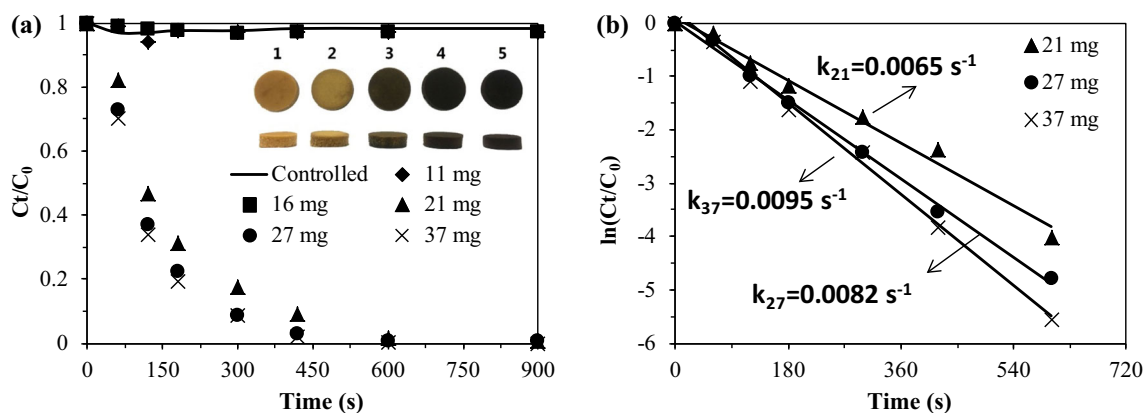


Figure 4 Effect of Pd loading amount on the foams on the hydrogenation of 3-NP (Pd(II) sorption process: foam mass, $255 \pm 10 \text{ mg}$; flow rate, 30 mL min^{-1} ; C_0 (Pd(II)), $10\text{--}50 \text{ mg L}^{-1}$. 3-NP hydrogenation: C_0 (3-NP), 50 mg L^{-1} ; volume, 0.1 L ; pH (unadjusted), 2.861 ; flow rate, 50 mL min^{-1} ; C_{HCOOH} ,

0.2%): **a** C_t/C_0 versus reaction time; **b** $\ln(C_t/C_0)$ versus reaction time. The inset in (a) shows the photographs of the catalysts loaded with different amounts of Pd (increasing in the order from 1 to 5); the controlled experiment corresponds to the blank (foam without Pd).

sorbed nitrophenol during the reaction is just non-detectable. Indeed, the k_{Pd} calculated for AP/Pd_{37mg} ($0.25 \text{ s}^{-1} \text{ g}^{-1}$) is much lower than that of AP/Pd_{27mg} ($0.30 \text{ s}^{-1} \text{ g}^{-1}$) and AP/Pd_{21mg} ($0.32 \text{ s}^{-1} \text{ g}^{-1}$). The excessive loading of the support with catalytic metal (and further metal nanoparticles) may lead to agglomeration of particles with lower accessibility and less rationale use of the metal catalyst. Indeed, a previous study showed that overloading Pd(II) on PEI particles resulted in large aggregates [36]. To maintain a high value for both k and k_{Pd} , AP/Pd_{27 mg} foam was chosen for further experiments.

Effect of flow rate during Pd sorption on catalytic performance

The recirculation-mode system proposed for metal loading in this study requires a specific analysis of sorption kinetics regarding the necessity to force the solution to flow through the sorbent and to ensure the metal ions can be well dispersed on the foams [45, 46]. A slow flow rate (FL) may easily lead to an accumulation of Pd(II) at the upper layer of the cylinder and to longitudinal metal gradient along the foam packing. Figure 5a shows that a higher flow rate produces catalysts with higher catalytic performance. The value of k (shown in Fig. 5b) increases significantly from 1.9×10^{-3} to $7.9 \times 10^{-3} \text{ s}^{-1}$ as the flow rate goes up from 5 to 30 mL min^{-1} . Further increasing the FL only leads to a slight improvement on the apparent rate constant, the beneficial effect of increasing flow velocity tends to stabilize the kinetic parameter. Therefore, an even higher FL was not

tested. The reason that causes this phenomenon should be that higher FL leads to more homogenous and less condensed distribution of Pd. This means that more Pd sites remain accessible; overloading due to heterogeneous dispersion may prevent sorption sites accessibility and may induce aggregation. The inset photograph in Fig. 5a shows the bottom of the cylinder. It is clear that at a low FL, the Pd loading is inhomogeneous with lower loading in the yellow (close to the raw color of the foams) area. This inevitably leads to Pd overloading in other part and consequently to less accessible Pd sites. Therefore, a FL of 50 mL min^{-1} was used for Pd(II) loading process in further experiments.

Effect of foam height during Pd sorption on catalytic performance

The effect of foam height was studied using different masses of foams with the same diameter (i.e., 2.43 cm). The masses of the foams are 175, 255 and 313 mg, and their corresponding measured thicknesses are 0.58, 0.85 and 1.06 cm, respectively. The values of Pd(II) loading amount on the foams are very close, which are 26.1, 27.2 and 27.7 mg g^{-1} , respectively. Because the same amount of palladium (volume and concentration) has been circulated through the foams of different heights, the density of Pd decreases with increasing foam depth. Figure S10 (see SI) shows that increasing the foam thickness does not affect the hydrogenation efficiency; the recirculation mode may explain this result. However, the comparison of the apparent rate constants shows a

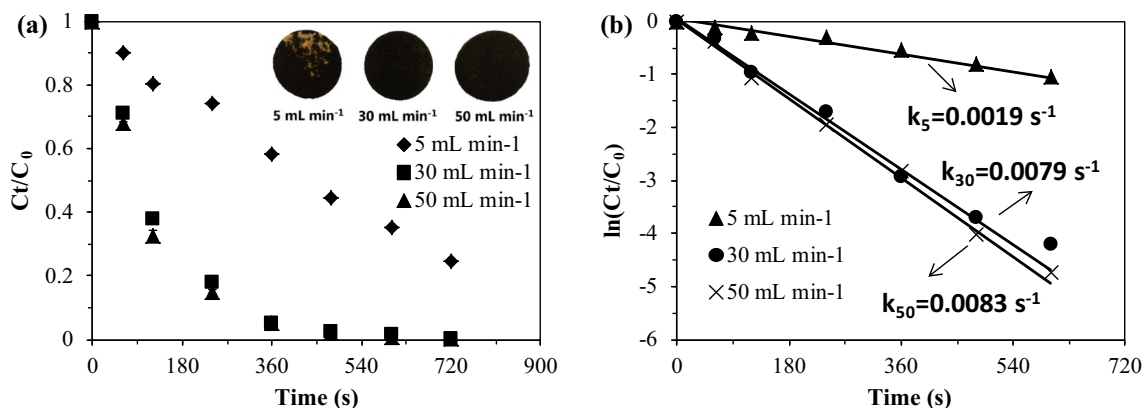


Figure 5 Effect of flow rate applied for Pd(II) sorption on the hydrogenation of 3-NP (Pd(II) sorption process: foam mass, $255 \pm 10 \text{ mg}$; C_0 (Pd(II)), 28 mg L^{-1} . 3-NP hydrogenation: Pd amount, 27 mg; volume, 0.1 L; C_0 (3-NP), 50 mg L^{-1} ; pH

(unadjusted), 2.86; flow rate, 50 mL min^{-1} ; $C_{(\text{HCOOH})}$, 0.2%): **a** C_t/C_0 versus reaction time; **b** $\ln(C_t/C_0)$ versus reaction time. The inset in (a) shows the photographs of the catalysts prepared by different flow rates.

higher relative catalytic activity for the thinner foam (thickness: 0.85 cm). The less dense Pd distribution associated with the foam thickness increase may thus result in (a) the formation of fewer aggregates of Pd nanoparticles, and (b) the increase in hydrogenation performance. However, increasing the depth of the catalytic foam does not enhance catalytic performance. This result can be partially explained by a change in the effective flow velocity (permeate flux) in the catalyst module. The amount of water passing through these foams with different thicknesses at a speed of 50 mL min⁻¹ for 1 min was recorded for different foam depths. The volume passed through the foam decreases from 49.8 ± 0.8 mL to 47.8 ± 0.4 mL and to 41.1 ± 0.3 mL for depths increasing according 0.58 cm, 0.85 cm and 1.06 cm, respectively. Increasing the depth of the catalytic foam modulates the admissible flow rate under selected experimental conditions.

The effect of foam thickness could be attributed to a variable yield in the reduction of the Pd(II) in the foam. The XPS analysis was performed on grinded sample reflecting the average characterization of the foam. Complementary analysis would be probably necessary for evaluating the effective impact of this potential heterogeneity. The mode of immobilization of Pd(II) by recirculation at high flow rate the metal-containing solutions of low concentrations allows maintaining a relatively homogeneous distribution of metal ions in the whole volume of the foam (as confirmed by the cartography of Pd (Figure S4, see SI).

Effect of solution pH and HCOOH concentration on catalytic performance

The solution pH may affect the catalytic reaction by changing the surface charge and the dissociation of both the substrate and the hydrogen donor. The pK_a values of primary, secondary and tertiary amine groups on PEI are 4.5, 6.7 and 11.6, respectively [47], while that of formic acid is 3.75 [48]. Figure S11a shows that degradation kinetics overlap when the value of initial pH is 3 or 4. Whereas when the initial pH decreases to pH 2 or increases to pH 5, the degradation rate significantly decreases. In addition, under these unfavorable conditions, the residual concentration of 3-NP decreases but does not reach a plateau within selected contact time. The value of k calculated for pH 2 is 3.2 × 10⁻³ s⁻¹ and 3.3 × 10⁻³ s⁻¹ for pH 5, which are much lower than

those of pH 3 and pH 4 (8.3 × 10⁻³ s⁻¹ and 8.2 × 10⁻³ s⁻¹, respectively). One plausible explanation can be the pH dependence of the electrostatic interaction between formic acid/formate and the catalyst surface [34]. A higher solution pH makes the catalyst surface more negative and inhibits the binding of formate (HCOO⁻) anions, while at low pH, the competition of competitor ions (brought by sulfuric acid for pH adjustment) may also decrease the binding of HCOO⁻.

The effect of the concentration of HCOOH was studied to select the optimal amount of HCOOH for 3-NP hydrogenation. The concentration of 3-NP was fixed at 50 mg L⁻¹, while that of HCOOH varied from 0.025% w/w to 0.4% w/w (corresponding to molar ratio of HCOOH/3-NP of 20–320) (Fig. S11b). At low formic acid concentration (i.e., lower than 0.1% w/w), the catalytic efficiency and the rate of 3-NP conversion strongly decrease. Increasing the concentration of HCOOH above 0.2% w/w does not significantly influence the catalytic activity. Thus, a HCOOH/3-NP molar ratio of 160 (0.2% w/w of HCOOH for 3-NP concentration close to 50 mg L⁻¹) was chosen for further study. These conditions correspond to a strong excess of hydrogen donor and a negligible variation in its concentration during the catalytic reaction; this may explain that the kinetic profile can be modeled using the pseudo-first-order rate equation.

Effect of flow rate during catalytic test

The overall hydrogenation efficiencies are very similar at all flow rates (data not shown). However, the apparent rate constant, shown in Fig. 6a, significantly increases with increasing the flow rate. In the mode of recirculation, a slow flow rate reduces the amount of wastewater to be treated in a given time. In this case, a higher flow rate (i.e., a shorter contact time) may be generally preferred for a better catalytic performance. Therefore, in further studies, 60 mL min⁻¹ was chosen as the optimum flow rate as increasing the flow rate to 70 mL min⁻¹ showed no significant difference.

Turnover frequency (TOF) and recyclability of the catalyst

Besides the high catalytic activity and ease of recovery, a high catalytic stability is another highly

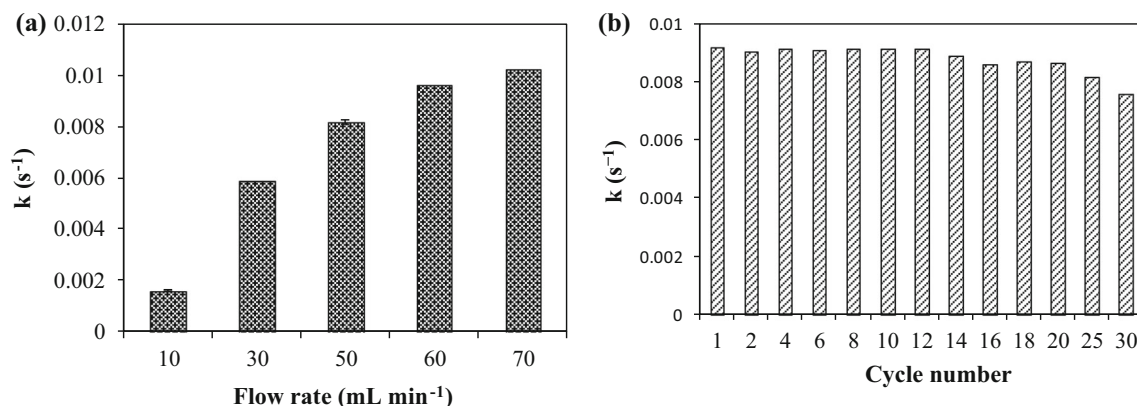


Figure 6 **a** Effect of flow rate on the hydrogenation of 3-NP (Pd amount: 27 mg; C_0 (3-NP): 50 mg L⁻¹; $C_{(\text{HCOOH})}$: 0.2%); **b** reuse of the catalyst for 3-NP hydrogenation (Pd amount: 27.3 mg; C_0 (3-NP): 50 mg L⁻¹; flow rate: 60 mL min⁻¹; $C_{(\text{HCOOH})}$: 0.2%).

required property for practical application. A reuse test was carried out over 30 cycles using AP/Pd catalyst. Owing to the specificity of the recirculation sorption system, separation process is not necessarily required; the foam catalyst was washed using 100 mL of water and reused directly in the next round by replacing the treated solution with a freshly prepared 3-NP solution. This should be advantageous in terms of easiness for practical applications. The results shown in Fig. 6b indicate that the catalytic activity of the Pd nanoparticles stabilized on AP foams maintains unchanged for 14 successive cycles; significant decrease only appears after 20 cycles. This confirms that AP/Pd foams are stable and reusable at least for 20 cycles. In most cases, the loss of catalytic activity is primarily due to metal leaching or support degradation. Indeed, the Pd loading amount of the catalysts determined by H₂SO₄-H₂O₂ digestion before and after 30 cycles is reduced by from 25.4 to 23.3 mg (8.3% loss, shown in Table S3, see SI). The metal loss is partially caused by the support loss; mass loss of the catalyst before and after the 30 cycles is found to be 3.89%. Despite these facts, the catalytic activity of AP/Pd catalyst at 30th cycle remains acceptable; actually, the loss on rate coefficient at the last cycle does not exceed 18%. This can be explained by the well dispersion of Pd nanoparticles on AP foams even after consecutive cycles; only a few aggregates of the nanoparticles are observed in the TEM image (shown in Figure S12, see SI) and the mean size measured is 8.00 ± 2.08 nm, which is close to the value observed on the raw catalyst (i.e., 7.61 ± 1.93 nm). The XPS analysis of recycled catalyst also confirmed minimal changes compared to

original catalyst (Figures S7 and S8 and Table S1, see SI). Another possible reason could be the partial decrease in the fraction of Pd effectively reduced on the catalyst (from 44 to 37%).

Table 2 compares the catalytic performance of AP/Pd foams with catalysts reported in the literature for the hydrogenation of nitrophenol compounds (including 3-NP and 4-NP). Although it is not appropriate directly comparing 3-NP and 4-NP hydrogenation rate coefficients, many papers have confirmed that the catalytic rate constants for hydrogenation of nitrophenols follow the order: 4-NP > 2-NP > 3-NP [49–53]. This could be due to the higher acidity of 4-NP compared with other NPs (i.e., $\text{p}K_{\text{a}}(4\text{-NP}) > \text{p}K_{\text{a}}(2\text{-NP}) > \text{p}K_{\text{a}}(3\text{-NP})$). This is directly correlated to the better resonance stability of 4-nitrophenolate ions than those of 2- and 3-nitrophenolate, as reported by Nguyen et al. [54]. Therefore, if the value of rate constant for 3-NP hydrogenation by AP/Pd is higher than that for 4-NP by another catalyst, it is reasonable concluding on the higher efficiency of AP/Pd compared with the reference material. When treating 100 mL of 50 mg L⁻¹ 3-NP solution, the rate constant is slightly lower than Pd/silica [55], but very competitive compared to other catalysts [56–61]. The outstanding catalytic activity should be due to high amount of Pd loaded and fine dispersion of Pd nanoparticles. Moreover, when compared to Pd nanoparticles supported on a similar material (algal biomass beads [36]), the rate constant significantly increases. This is owing to the much more porous structure of AP foams and the unique treatment system (fixed-bed column system) that allows more effective mass transfer process. In

Table 2 Comparison of the catalytic hydrogenation of nitrophenol compounds (3- and 4-NP) using various catalysts

Composites	Type	NP	$k \times 10^3$ (s ⁻¹) ^a	$n_{\text{nitrophenol}}$ (mmol)	n_{metal} (mmol)	TOF (mmol mmol ⁻¹ min ⁻¹)	References
HABA/PEI (Pd)	Millimeter-scale beads	3-NP	0.022	—	—	—	[36]
Ni-Pt	Nanoparticles	4-NP	1.93	—	—	—	[56]
PNIPA gels (Ag)	Core-Shell nanoparticles	4-NP	3.50	—	—	—	[57]
Pd/polypyrrole	Nanocapsules	4-NP	8.87	—	—	—	[58]
Pd/Fe ₃ O ₄ @SiO ₂ @KCC-1	Nanocomposites	4-NP	1.96	—	—	—	[59]
Pd/nano-silica	Nanocomposites	4-NP	8.00	—	—	—	[60]
Pd/polyelectrolyte brushes	Nanocomposites	4-NP	4.40	—	—	—	[61]
Pd/micro-gels	Nanocomposites	4-NP	1.50	—	—	—	[61]
Pd/RGO ^b	Nanocomposites	4-NP	—	1	1.2	6.38	[64]
Pd ₁ (Co) ₁₅ /RGO	Nanocomposites	4-NP	—	1	0.5	396	[64]
Pd/silica	Nanocomposites	4-NP	11.80	—	—	1.126	[55]
Concave Pd-TNCs	Nanoparticles	4-NP	—	2×10^{-4}	1.5×10^{-4}	0.148	[63]
Flat Pd-TNCs	Nanoparticles	4-NP	—	2×10^{-4}	1.5×10^{-4}	0.095	[63]
Solid Pd/Fe ₃ O ₄	Nanocomposites	4-NP	—	2.16	0.02	0.01	[62]
Hollow Pd/Fe ₃ O ₄	Nanocomposites	4-NP	—	2.16	0.02	0.015	[62]
Pd/graphene	Nanohybrids	4-NP	2.35	2.9×10^{-4}	5×10^{-8}	13.63	[65]
Tryptophan-Cu-Ag	Nanoparticles	4-NP	39.6	^c	—	—	[53]
Tryptophan-Cu-Ag	Nanoparticles	3-NP	23.0	—	—	—	[53]
Au nanoparticles	Nanoparticles	3-NP	13.2	3×10^{-4}	2.6×10^{-5}	9.1	[52]
Ni-Au nanocatalyst	Nanocomposites	3-NP	10	0.2	0.0091	0.22	[51]
Au/activated coke	Micron-scale powder	3-NP	6.6	—	—	0.18	[50]
AP/Pd	Foam	3-NP	9.70	0.036	0.25	0.082	This study
AP/Pd	Foam	3-NP	1.53	0.50	0.25	0.184	This study

^ak: apparent rate constant^bRGO: reduced graphene oxide^cIdentical (hydrogen donor/substrate ratio)

order to further compare the catalytic activity of AP/Pd foams with other catalysts reported previously, the turnover frequency (TOF, defined as the number of 3-NP molecules per metallic Pd per minute based on the total mass of metallic Pd, i.e., mmol mmol⁻¹ min⁻¹) of AP/Pd was deduced from apparent rate constant (k). The value of TOF is 0.184 mmol mmol⁻¹ min⁻¹ when the concentration of 3-NP is 700 mg L⁻¹, which is higher to those of Pd/Fe₃O₄ composites [62] and Pd-TNCs [63], but much lower than other catalysts [55, 64, 65]. However, it is noteworthy that, in this study, a much less poisonous hydrogen donor (HCOOH) compared to NaBH₄, which was previously used in the cited literature. In addition, all the catalyst composites listed are all nanoscale, which could lead to difficulty for recovery or poor stability. For example, Xue et al. [58] observed a decrease on catalytic activity when reusing Pd/polypyrrole nanocapsules after the first

hydrogenation. Similarly, another study [66] showed that the catalytic activity of Pd/CuO nanoparticles decreased gradually during 6 cycles. Wang et al. [62] reported that the catalytic activity of Pd/Fe₃O₄ spheres decreased significantly in subsequent runs; the conversion decreased from 85% in the first cycle to 22% in the fifth cycle. These results indicate that the catalyst undergone gradual and relatively fast deactivation. They attributed this deactivation to the interaction between the aminophenol molecules and the Pd nanoparticles. The lone pair electrons on the N atom in aminophenol coordinate to the 4d orbitals of palladium atoms; therefore, the catalytically active sites of the Pd nanoparticles are progressively poisoned. The abundant amine groups on the foams, the large size of the support, and the uniqueness of the treatment system that does not require solid-separation process help the stability of AP/Pd catalyst for reuse in successive cycles. Therefore, compared to

these nanoscale catalyst composites, the main advantages of AP/Pd foams are: (1) no requirement of separation process after treatment, (2) high stability and (3) flexibility concerning the treatment system. Indeed, the foams can be easily applied in fixed-bed system, using recirculation mode or one-pass mode (see “Tests in dynamic systems (one-pass mode)” section).

Synthesis of AP/Pd and pathway of 3-NP hydrogenation

Figure 7 shows the mechanism of preparation of AP/Pd catalysts and suggests the reaction pathway for the 3-NP hydrogenation by HCOOH. The pK_a of carboxyl groups on alginate is approximately 4, while those of primary, secondary and tertiary amine groups on PEI were reported as 4.5, 6.7 and 11.6, respectively [47]. Therefore, a simple pH control makes possible the cross-linking between negatively charged carboxyl groups on alginate and positively charged amine groups on PEI. Besides, to improve the stability of the foams, the free PEI on alginate was further cross-linked with GA as a post-treatment. In this case, alginate constitutes the support for PEI-GA; meanwhile, the PEI-GA cross-linking, in turn,

improves the stability of the composite foam. This double cross-linking avoids the collapse of the porous structure of the foams. Unlike the conventional methods for preparing alginate-based foams, AP foam does not require strict drying conditions. An air-drying process barely shrinks the porous material. The high percolating property allows palladium solution passing through the material in a fixed-bed column system with a high flow rate, enhancing homogeneous Pd dispersion. After metal reduction, Pd nanoparticles can be firmly immobilized to abundant amine groups on AP foams, contributing to the high stability of the catalyst when reusing. This is consistent with the result from the “recyclability of the catalyst” section. To conclude, AP support plays an essential role in the dispersion and stability of Pd nanoparticles:

- The surface of AP is positively charged due to the abundant amine groups on PEI, while Pd nanoparticles are generally negatively charged. Thus, Pd nanoparticles can be firmly immobilized through electrostatic interaction.
- The presence of alginate helps in distributing amine groups to the whole mass of AP foam, improving the stability of the composite foam.

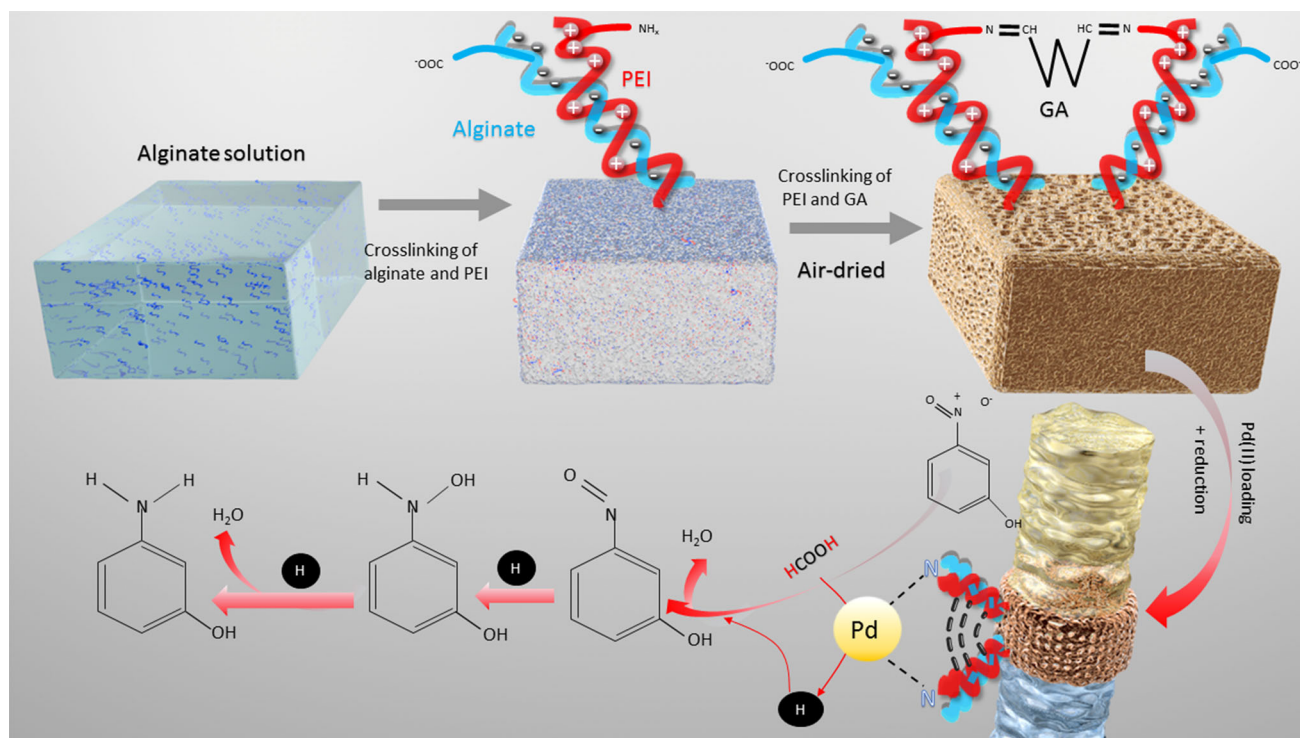


Figure 7 Mechanism of preparation of AP/Pd catalysts and proposed reaction pathway for the 3-NP hydrogenation by HCOOH.

preventing the aggregation of Pd nanoparticles trapped by amine groups.

- (c) The unique structure (porous foam) allows the application in fixed-bed column system. Thus, when loading metal ions, the high flow rate (such as 50 mL min^{-1}) can be applied and is beneficial to the good dispersion of Pd.

The critical impact of foam depth could be assigned to the potential impact of mass transfer on both metal sorption, metal reduction and further catalytic reaction. This impact is clearly minimized when low metal concentrations are used in the immobilization process (homogeneous metal dispersion, minimization of agglomeration effects) and for the hydrogenation reaction (avoiding preferential channels). The effect of foam depth on metal reduction (carried out in batch process) is not optimized and would require additional development.

The decomposition of formic acid was reported to proceed through either the carboxyl (COOH) route or formate (HCOO) route [67]. The former process begins with the C–H bond dissociation and continues with the OH one, while the latter one starts with the O–H bond breaking, forming stable bidentate formate HCOO_B intermediate. The presence of Pd nanoparticles induces the capture of hydrogen from HCOOH and thus assists the dissociation of HCOOH. Thereafter, the H^\bullet radical attacks the positively charged nitrogen of 3-NP, catalyzing the hydrogenation of 3-nitrophenol to 3-aminophenol.

Tests in dynamic systems (one-pass mode)

To evaluate the catalytic performance of AP/Pd in the one-pass mode, the continuous reaction was carried out using the following experimental conditions: 100 mL of solutions with different initial 3-NP and HCOOH concentrations (molar ratio of HCCOH *vs.* 3-NP was maintained at 160) was fed through the catalytic foams at different flow rates. The effluent was collected out of the reactor in fractions (4 mL for each). The outlet solutions look clear with generation of micro-bubbles; this indicates the excess HCOOH is coming out along with 3-AP. As shown in Fig. 8, when the flow rate is lower than 10 mL min^{-1} , the 3-NP concentration of the effluent is lower than 0.5 mg L^{-1} , regardless of the initial concentration. However, for an initial 3-NP concentration of 150 mg L^{-1} or 200 mg L^{-1} , as the flow rate increases

to 20 mL min^{-1} (or more), the reaction is not complete; the 3-NP concentration of effluents increases with increasing feed volume. An explanation may be the lack of enough Pd nanoparticles for treating the substrate for selected residence time. This could be also explained by the progressive poisoning of AP/Pd catalysts by acidic species. Deng et al. [68] reported that supported Ru catalysts were poisoned when the concentration of formic acid or formate was higher than 10 mmol L^{-1} . The catalytic oxidation of formic acid produces poisoning species, which may block the active sites of Pd catalyst. As described above, formic acid decomposition proceeds via either the formate (HCOO) or carboxyl (COOH) intermediate routes. Yoo et al. observed that 60–82% of H_2 is produced via HCOO intermediate on Pd, indicating that the active sites were more likely blocked by COOH intermediate [69]. Moreover, the carboxyl intermediate route produces CO, which could be another source of poisoning [69]. To regenerate the catalyst, a washing step was conducted to desorb the poisoning compounds by passing 40 mL of water; thereafter, the 3-NP solution was continuously fed through the regenerated catalyst. Results shown in Fig. 8d demonstrate that the catalytic performance of AP/Pd foams can be easily recovered after washing with water, regardless of the feeding speed: Poisoning species are weakly bound to AP/Pd foams (easy elution).

Conclusions

The macroporous and stable alginate and polyethyleneimine (AP) foams synthesized in this study show high recovery efficiency for Pd(II) from acidic solution: sorption capacity up to 224 mg Pd g^{-1} at pH 1 (with high stability of bound metal). The loaded Pd(II) can be partially reduced into Pd(0) using hydrazine hydrate ($\text{N}_2\text{H}_4\cdot\text{H}_2\text{O}$) in alkaline solution (based on XPS analysis, the yield of reduction is close to 44%). The average size of Pd nanoparticles is close to 7–8 nm (measured by TEM). Pd-supported catalytic foam is successfully applied for 3-NP hydrogenation using HCOOH as hydrogen donor in a recirculation mode (batch mode). The best Pd(II) loading condition corresponds, for a 255 mg amount of foam, to an initial Pd(II) concentration of 28 mg L^{-1} at pH 1 (volume: 1 L) and flow rate of

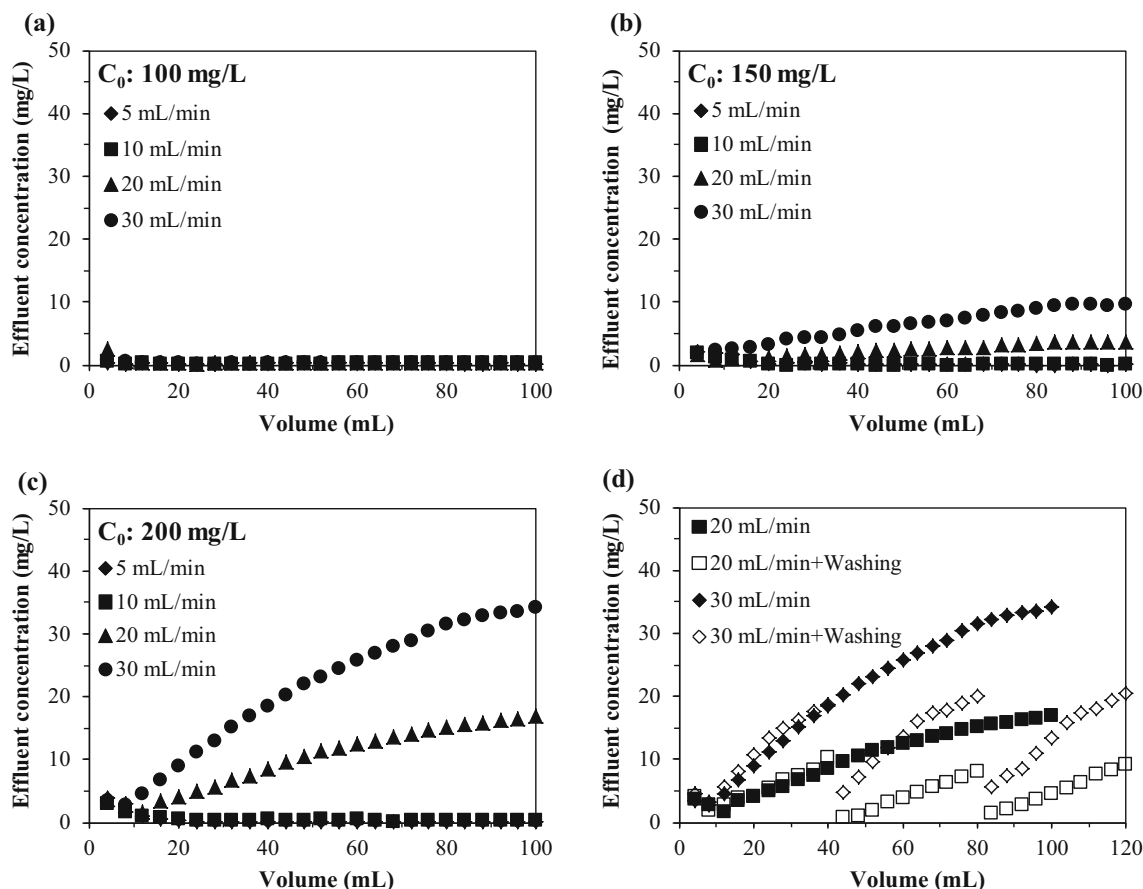


Figure 8 Hydrogenation of 3-NP in one-pass mode (Pd amount: 27.2 ± 0.3 mg; C_0 (3-NP): 100–200 mg L⁻¹; flow rate: 5–30 mL min⁻¹).

50 mL min⁻¹. In the case of 3-NP hydrogenation, best operating conditions correspond to:

- (a) Initial pH: 3–4.
- (b) Flow rate: 60 mL min⁻¹.
- (c) HCOOH/3-NP molar ratio: 160.

Under selected experimental conditions, the kinetic profiles can be modeled using the pseudo-first order rate equation. The catalyst can be recycled, used for 30 successive cycles, and it appears that the catalytic activity decreases after 20 cycles. In the one-pass mode (dynamic operating), the progressive poisoning of the catalyst decreases the hydrogenation efficiency; however, washing the catalyst with water allowed readily restoring catalytic activity.

The catalytic foams offer very promising perspectives for developing stable supports with highly percolating properties, confinement of catalytic nanoparticles, reusable and easy to regenerate. The enhancement of catalytic activity will require improving the efficiency of metal reduction (limited

here to 44%), and the recycling/reuse could be enhanced by introducing a new reduction step after catalyst washing (currently under investigation).

Acknowledgements

S. Wang (CSC, Grant No. 20156660002) and Y. Mo (CSC, Grant No. 201708450080) acknowledge the China Scholarship Council for providing PhD fellowship. E. Rodríguez-Castellón thanks to project RTI2018-099668-B-C22 (Ministerio de Ciencia, Innovación y Universidades of Spain) project UMA18-FEDERJA-126 of Junta de Andalucía (Spain) and FEDER fund.

Electronic supplementary material: The online version of this article (<https://doi.org/10.1007/s10853-019-04099-y>) contains supplementary material, which is available to authorized users.

References

- [1] Gu J, Hu CS, Zhang WW, Dichiara AB (2018) Reagentless preparation of shape memory cellulose nanofibril aerogels decorated with Pd nanoparticles and their application in dye discoloration. *Appl Catal B* 237:482–490
- [2] Islam M, Mondal P, Roy AS, Tuhina K (2010) Catalytic hydrogenation of various organic substrates using a reusable polymer-anchored palladium(II) complex. *J Mater Sci* 45:2484–2493. <https://doi.org/10.1007/s10853-010-4220-2>
- [3] Cardenas-Lizana F, Keane MA (2013) The development of gold catalysts for use in hydrogenation reactions. *J Mater Sci* 48:543–564. <https://doi.org/10.1007/s10853-012-6766-7>
- [4] Sogukomerogullari HG, Karatas Y, Celebi M, Gulcan M, Sonmez M, Zahmakiran M (2019) Palladium nanoparticles decorated on amine functionalized graphene nanosheets as excellent nanocatalyst for the hydrogenation of nitrophenols to aminophenol counterparts. *J Hazard Mater* 369:96–107
- [5] Xia J, Zhang L, Fu Y, He G, Sun X, Wang X (2018) Nitrogen-doped carbon black supported NiCo_2S_4 catalyst for hydrogenation of nitrophenols under mild conditions. *J Mater Sci* 53:4467–4481. <https://doi.org/10.1007/s10853-017-1852-5>
- [6] Zhang YM, Cao YH, Chen D, Cui PL, Yang J (2018) Ionic liquid assisted synthesis of palladium nanoclusters for highly efficient formaldehyde oxidation. *Electrochim Acta* 269:38–44
- [7] Wołowicz A, Hubicki Z (2014) Adsorption characteristics of noble metals on the strongly basic anion exchanger Purolite A-400TL. *J Mater Sci* 49:6191–6202. <https://doi.org/10.1007/s10853-014-8333-x>
- [8] Zhang Z, Sebe G, Wang XS, Tam KC (2018) Gold nanoparticles stabilized by poly(4-vinylpyridine) grafted cellulose nanocrystals as efficient and recyclable catalysts. *Carbohydr Polym* 182:61–68
- [9] Li J, Bai X (2016) Ultrasonic synthesis of supported palladium nanoparticles for room-temperature Suzuki-Miyaura coupling. *J Mater Sci* 51:9108–9122. <https://doi.org/10.1007/s10853-016-0164-5>
- [10] Deng C, Li Y, Sun W, Liu F, Zhang Y, Qian H (2019) Supported AuPd nanoparticles with high catalytic activity and excellent separability based on the magnetic polymer carriers. *J Mater Sci* 54:11435–11447. <https://doi.org/10.1007/s10853-019-03701-7>
- [11] Wang H, Wan Y (2009) Synthesis of ordered mesoporous Pd/carbon catalyst with bimodal pores and its application in water-mediated Ullmann coupling reaction of chlorobenzene. *J Mater Sci* 44:6553–6562. <https://doi.org/10.1007/s10853-009-3612-7>
- [12] Wilson OM, Knecht MR, Garcia-Martinez JC, Crooks RM (2006) Effect of Pd nanoparticle size on the catalytic hydrogenation of allyl alcohol. *JACS* 128:4510–4511
- [13] Gawade AB, Nakhate AV, Yadav GD (2018) Selective synthesis of 2,5-furandicarboxylic acid by oxidation of 5-hydroxymethylfurfural over MnFe_2O_4 catalyst. *Catal Today* 309:119–125
- [14] Das R, Sypu VS, Paumo HK, Bhaumik M, Maharaj V, Maity A (2019) Silver decorated magnetic nanocomposite (Fe_3O_4 @PPy-MAA/Ag) as highly active catalyst towards reduction of 4-nitrophenol and toxic organic dyes. *Appl Catal B* 244:546–558
- [15] Zhao YQ, Wu ZF, Wang YQ, Yang C, Li YX (2017) Facile fabrication of polystyrene microsphere supported gold-palladium alloy nanoparticles with superior catalytic performance for the reduction of 4-nitrophenol in water. *Colloids Surf. A* 529:417–424
- [16] Palchoudhury S, Lead JR (2014) A facile and cost-effective method for separation of oil-water mixtures using polymer-coated iron oxide nanoparticles. *Environ Sci Technol* 48:14558–14563
- [17] Rosch JG, Winter H, DuRoss AN, Sahay G, Sun C (2019) Inverse-micelle synthesis of doxorubicin-loaded alginate/chitosan nanoparticles and in vitro assessment of breast cancer cytotoxicity. *Colloid Interface Sci Commun* 28:69–74
- [18] Ben Hammouda S, Adhoum N, Monser L (2016) Chemical oxidation of a malodorous compound, indole, using iron entrapped in calcium alginate beads. *J Hazard Mater* 301:350–361
- [19] An B, Lee H, Lee S, Lee SH, Choi JW (2015) Determining the selectivity of divalent metal cations for the carboxyl group of alginate hydrogel beads during competitive sorption. *J Hazard Mater* 298:11–18
- [20] Carvalho AGD, Machado MTD, Barros H, Cazarin CBB, Marostica MR, Hubinger MD (2019) Anthocyanins from jussara (*Euterpe edulis Martius*) extract carried by calcium alginate beads pre-prepared using ionic gelation. *Powder Technol* 345:283–291
- [21] Zhao J, Zhu YW, He GW et al (2016) Incorporating zwitterionic graphene oxides into sodium alginate membrane for efficient water/alcohol separation. *ACS Appl Mater Interfaces* 8:2097–2103
- [22] Ma YL, Qi PF, Ju JP et al (2019) Gelatin/alginate composite nanofiber membranes for effective and even adsorption of cationic dyes. *Compos B* 162:671–677
- [23] Post W, Jeoffroy E, Garcia SJ, van der Zwaag S (2019) Self-healing glass fiber reinforced polymer composites based on montmorillonite reinforced compartmented alginate fibers. *Polym Compos* 40:471–480

- [24] Eibak LEE, Hegge AB, Rasmussen KE, Pedersen-Bjergaard S, Gjelstad A (2012) Alginate and chitosan foam combined with electromembrane extraction for dried blood spot analysis. *Anal Chem* 84:8783–8789
- [25] Saha S, Pal A, Kundu S, Basu S, Pal T (2010) Photochemical green synthesis of calcium-alginate-stabilized Ag and Au nanoparticles and their catalytic application to 4-nitrophenol reduction. *Langmuir* 26:2885–2893
- [26] Kuang Y, Du JH, Zhou RB, Chen ZL, Megharaj M, Naidu R (2015) Calcium alginate encapsulated Ni/Fe nanoparticles beads for simultaneous removal of Cu(II) and monochlorobenzene. *J Colloid Interface Sci* 447:85–91
- [27] Chitichirovsky M, Lin Y, Ouchaou K et al (2012) Dramatic effect of the gelling cation on the catalytic performances of alginate-supported palladium nanoparticles for the Suzuki–Miyaura reaction. *Chem Mater* 24:1505–1510
- [28] Kumar M, Vijayakumar G, Tamilarasan R (2019) Synthesis, characterization and experimental studies of nano Zn–Al–Fe₃O₄ blended alginate/Ca beads for the adsorption of rhodamine B. *J Polym Environ* 27:106–117
- [29] Wang S, Vincent T, Faur C, Guibal E (2018) A comparison of palladium sorption using polyethylenimine impregnated alginate-based and carrageenan-based algal beads. *Appl Sci Basel* 8:264
- [30] Loges B, Boddien A, Junge H, Beller M (2008) Controlled generation of hydrogen from formic acid amine adducts at room temperature and application in H₂/O₂ fuel cells. *Angew Chem Int Ed* 47:3962–3965
- [31] Gowda DC, Gowda S (2000) Formic acid with 10% palladium on carbon: a reagent for selective reduction of aromatic nitro compounds. *Indian J Chem Sect B* 39:709–711
- [32] Zhang Y, He X, Ouyang J, Yang H (2013) Palladium nanoparticles deposited on silanized halloysite nanotubes: synthesis, characterization and enhanced catalytic property. *Sci Rep* 3:2948
- [33] Vincent T, Guibal E (2003) Chitosan-supported palladium catalyst. 3. Influence of experimental parameters on nitrophenol degradation. *Langmuir* 19:8475–8483
- [34] Javaid R, Kawasaki S-i, Suzuki A, Suzuki TM (2013) Simple and rapid hydrogenation of p-nitrophenol with aqueous formic acid in catalytic flow reactors, Beilstein. *J Org Chem* 9:1156–1163
- [35] Vincent T, Krys P, Jouannin C, Gaumont A-C, Dez I, Guibal E (2013) Hybrid macroporous Pd catalytic discs for 4-nitroaniline hydrogenation: contribution of the alginate-tetraalkylphosphonium ionic liquid support. *J Organomet Chem* 723:90–97
- [36] Wang S, Vincent T, Faur C, Rodriguez-Castellon E, Guibal E (2019) A new method for incorporating polyethylenimine (PEI) in algal beads: high stability as sorbent for palladium recovery and supported catalyst for nitrophenol hydrogenation. *Mater Chem Phys* 221:144–155
- [37] Perez-Coronado AM, Calvo L, Alonso-Morales N, Heras F, Rodriguez JJ, Gilarranz MA (2016) Multiple approaches to control and assess the size of Pd nanoparticles synthesized via water-in-oil microemulsion. *Colloids Surf A* 497:28–34
- [38] Simonsen SB, Chorkendorff I, Dahl S, Skoglundh M, Helveg S (2016) Coarsening of Pd nanoparticles in an oxidizing atmosphere studied by in situ TEM. *Surf Sci* 648:278–283
- [39] Zhang C, Leng Y, Jiang P, Li J, Du S (2017) Immobilizing palladium nanoparticles on nitrogen-doped carbon for promotion of formic acid dehydrogenation and alkene hydrogenation. *Chem Sel* 2:5469–5474
- [40] Kim Y-H, Ogata T, Nakano Y (2007) Kinetic analysis of palladium(II) adsorption process on condensed-tannin gel based on redox reaction models. *Water Res* 41:3043–3050
- [41] Wang S, Vincent T, Roux J-C, Faur C, Guibal E (2017) Pd(II) and Pt(IV) sorption using alginate and algal-based beads. *Chem Eng J* 313:567–579
- [42] Miller KJ, Kitagawa TT, Abu-Omar MM (2001) Kinetics and mechanisms of methyl vinyl ketone hydroalkoxylation catalyzed by palladium(II) complexes. *Organometallics* 20:4403–4412
- [43] Baran T, Sargin I, Menten A, Kaya M (2016) Exceptionally high turnover frequencies recorded for a new chitosan-based palladium(II) catalyst. *Appl Catal A* 523:12–20
- [44] Jadbabaei N, Slobodjian RJ, Shuai D, Zhang H (2017) Catalytic reduction of 4-nitrophenol by palladium-resin composites. *Appl Catal A* 543:209–217
- [45] Guibal E, Cambe S, Bayle S, Taulemesse J-M, Vincent T (2013) Silver/chitosan/cellulose fibers foam composites: from synthesis to antibacterial properties. *J Colloid Interface Sci* 393:411–420
- [46] Wang S, Vincent T, Faur C, Guibal E (2017) Algal foams applied in fixed-bed process for lead(II) removal using recirculation or one-pass modes. *Mar Drugs* 15:315
- [47] Willner I, Eichen Y, Frank AJ, Fox MA (1993) Photinduced electron-transfer processes using organized redox-functionalized bipyridinium polyethyleneimine TiO₂ colloids and particulate assemblies. *J Phys Chem* 97:7264–7271
- [48] Harmsen JMA, Jelemensky L, Van Andel-Scheffer PJM, Kuster BFM, Marin GB (1997) Kinetic modeling for wet air oxidation of formic acid on a carbon supported platinum catalyst. *Appl Catal A* 165:499–509
- [49] Goyal A, Bansal S, Singhal S (2014) Facile reduction of nitrophenols: comparative catalytic efficiency of MFe₂O₄ (M = Ni, Cu, Zn) nano ferrites. *Int J Hydrog Energy* 39:4895–4908
- [50] Fu Y, Qin L, Huang D et al (2019) Chitosan functionalized activated coke for Au nanoparticles anchoring: Green

- synthesis and catalytic activities in hydrogenation of nitrophenols and azo dyes. *Appl Catal B* 255:117740
- [51] Qin L, Zeng Z, Zeng G et al (2019) Cooperative catalytic performance of bimetallic Ni–Au nanocatalyst for highly efficient hydrogenation of nitroaromatics and corresponding mechanism insight. *Appl Catal B* 259:118035
- [52] Zhang X, Qu Y, Shen W et al (2016) Biogenic synthesis of gold nanoparticles by yeast *Magnusiomyces ingens* LH-F1 for catalytic reduction of nitrophenols. *Colloids Surf A* 497:280–285
- [53] Meng YX, Gao HY, Li S, Chai F, Chen LH (2019) Facile fabrication of bimetallic Cu–Ag binary hybrid nanoparticles and their application in catalysis. *New J Chem* 43:6772–6780
- [54] Nguyen TB, Huang CP, Doong R-A (2019) Enhanced catalytic reduction of nitrophenols by sodium borohydride over highly recyclable Au@graphitic carbon nitride nanocomposites. *Appl Catal B* 240:337–347
- [55] Morere J, Tenorio MJ, Torralvo MJ, Pando C, Renuncio JAR, Cabanas A (2011) Deposition of Pd into mesoporous silica SBA-15 using supercritical carbon dioxide. *J Supercrit Fluids* 56:213–222
- [56] Ghosh SK, Mandal M, Kundu S, Nath S, Pal T (2004) Bimetallic Pt–Ni nanoparticles can catalyze reduction of aromatic nitro compounds by sodium borohydride in aqueous solution. *Appl. Catal. A* 268:61–66
- [57] Lu Y, Mei Y, Drechsler M, Ballauff M (2006) Thermosensitive core-shell particles as carriers for Ag nanoparticles: modulating the catalytic activity by a phase transition in networks. *Angew Chem Int Ed* 45:813–816
- [58] Xue Y, Lu X, Bian X, Lei J, Wang C (2012) Facile synthesis of highly dispersed palladium/polypyrrole nanocapsules for catalytic reduction of p-nitrophenol. *J Colloid Interface Sci* 379:89–93
- [59] Le X, Dong Z, Liu Y et al (2014) Palladium nanoparticles immobilized on core-shell magnetic fibers as a highly efficient and recyclable heterogeneous catalyst for the reduction of 4-nitrophenol and Suzuki coupling reactions. *J Mater Chem A* 2:19696–19706
- [60] Le X, Dong Z, Li X, Zhang W, Minhdong L, Ma J (2015) Fibrous nano-silica supported palladium nanoparticles: an efficient catalyst for the reduction of 4-nitrophenol and hydrodechlorination of 4-chlorophenol under mild conditions. *Catal Commun* 59:21–25
- [61] Mei Y, Lu Y, Polzer F, Ballauff M, Drechsler M (2007) Catalytic activity of palladium nanoparticles encapsulated in spherical polyelectrolyte brushes and core-shell microgels. *Chem Mater* 19:1062–1069
- [62] Wang H-Q, Wei X, Wang K-X, Chen J-S (2012) Controlled synthesis of magnetic Pd/Fe₃O₄ spheres via an ethylenediamine-assisted route. *Dalton Trans* 41:3204–3208
- [63] Fu G, Jiang X, Ding L et al (2013) Green synthesis and catalytic properties of polyallylamine functionalized tetrahedral palladium nanocrystals. *Appl. Catal. B* 138:167–174
- [64] Dong W, Cheng S, Feng C, Shang N, Gao S, Wang C (2017) Fabrication of highly dispersed Pd nanoparticles supported on reduced graphene oxide for catalytic reduction of 4-nitrophenol. *Catal Commun* 90:70–74
- [65] Wang Z, Xu C, Gao G, Li X (2014) Facile synthesis of well-dispersed Pd-graphene nanohybrids and their catalytic properties in 4-nitrophenol reduction. *RSC Adv* 4:13644–13651
- [66] Nasrollahzadeh M, Sajadi SM, Rostami-Vartooni A, Bagherzadeh M (2015) Green synthesis of Pd/CuO nanoparticles by Theobroma cacao L. seeds extract and their catalytic performance for the reduction of 4-nitrophenol and phosphine-free Heck coupling reaction under aerobic conditions. *J Colloid Interface Sci* 448:106–113
- [67] Ruppert AM, Jedrzejczyk M, Potrzebowska N et al (2018) Supported gold-nickel nano-alloy as a highly efficient catalyst in levulinic acid hydrogenation with formic acid as an internal hydrogen source. *Catal Sci, Technol*, p 8
- [68] Deng L, Zhao Y, Li J, Fu Y, Liao B, Guo Q-X (2010) Conversion of levulinic acid and formic acid into gamma-valerolactone over heterogeneous catalysts. *Chemsuschem* 3:1172–1175
- [69] Yoo JS, Zhao Z-J, Norskov JK, Studt F (2015) Effect of boron modifications of palladium catalysts for the production of hydrogen from formic acid. *ACS Catal* 5:6579–6586